Ruthenium-peptide conjugates for targeted phototherapy

Zhang, I.

5

Diastereomers of Ru-MRGDM complexes for photoactivated chemotherapy: synthesis and biological properties

In this work, three ruthenium-peptide conjugates ***[1]***Cl_2-***[3]***Cl_2 *were synthesized, by coordination of cis-*$[Ru(Ph_2phen)_2Cl_2]$ *with the three peptides Ac-MRGDM-*NH_2*, Ac-mrGdm-*NH_2*, and Ac-MrGdM-*NH_2*, respectively, where M, R and D are natural L-amino acids and m, r, d are unnatural D-amino acids. Due to the Δ/Λ chiral nature of octahedral ruthenium complexes bound to three bidentate chelating ligands, the complexes* ***[1]***Cl_2*–* ***[3]***Cl_2 *were obtained as pairs of diastereoisomers that were further separated by HPLC. Six diastereomers were isolated and fully characterized: Δ-****[1]***Cl_2*, Λ-****[1]***Cl_2*, Δ-****[2]***Cl_2**,** *Λ-****[2]***Cl_2*, Δ-****[3]***Cl_2 *and Λ-****[3]***Cl_2*. Upon irradiation with green light (515 nm) in water, all six diastereomers substituted their peptide for water molecules by an efficient two-step photoreaction (*Φ_{PS1} *= 0.15-0.26 and* Φ_{PS2} *= 0.0050-0.0092 respectively). They showed mild cytotoxicity (*EC_{50} *>30 μM) in the dark towards A549 human lung cancer cell lines in normoxia (21%* O_2*) or hypoxia (1%* O_2*), as well as towards A549 tumor spheroids, but after light activation up to 20× higher cytotoxicity (*EC_{50} *<7 μM) was observed. Most importantly, their photo index values were retained in hypoxic cells (PI up to 4.5), and no generation of ROS was detected. Considering their high photosubstitution quantum yield and low* $^1O_2$ *generation quantum yield, this series of complexes represent a set of highly efficient photoactivated chemotherapy (PACT) compounds. However, the replacement of natural L-amino acids by D-amino acids had a limited influence on the performance of the compounds, in terms of both photochemical and photobiological properties* in vitro.

This chapter will be submitted as a full paper: L. Zhang, H. Bronkhorst, Y. Husiev, L. Bretin and S. Bonnet*. *In preparation.*

5.1 Introduction

When tumors reach a certain size, compared with healthy tissues, the O_2 tension becomes very low in solid tumors due to inadequate oxygen delivery and high consumption of O_2 caused by high cell proliferating rates. This condition, which is called hypoxia, represents one of the important barriers for the anticancer action of a number of chemotherapy agents.[1-3] To adapt to the hypoxic environment of solid tumors, cancer cells also trigger a response, mostly *via* switching on hypoxia-inducible factors 1 and 2 (HIF1, HIF2).[4] The role of hypoxia and HIFs in reprogramming cancer cells by regulating the expression of multiple genes involved in angiogenesis, metabolic regulation, cancer cell invasion, and metastasis, etc.[3] make hypoxic solid tumors particularly resistant to many anticancer drugs. In particular, the efficacy of chemotherapy compounds that rely on the generation of reactive oxygen species (ROS) to be cytotoxic, for example photosensitizers used for photodynamic therapy (PDT), is strongly affected by hypoxia.[1, 5] In PDT tumor treatment, the photosensitizer molecule that absorbs light relies on either electron or energy transfer to O_2 present in the irradiated tissues, to generate cytotoxic ROS such as singlet oxygen ($^1O_2$) or superoxide radical ions ($O_2^{\bullet-}$). At low O_2 concentrations in the tumor tissues, such stimulation often fails, making PDT drugs lose their efficiency.[6, 7]

In order to overcome these limitations, an alternative light-triggered cancer treatment modality called photoactivated chemotherapy (PACT) has been developed, which is characterized by its oxygen-independent activation mechanism.[8] PACT relies on photocleavage reactions that release a coordinated molecule from a metal center, to generate local cytotoxicity. Depending on molecular design, either the released ligand or the uncaged metal-containing photoproduct may be cytotoxic.[9, 10] Many PACT compounds have been described,[11, 12] but those based on ruthenium(II) polypyridyl complexes have emerged as particularly promising.[13, 14] These complexes carry one or more labile ligands that are photosubstituted upon excitation by visible light.[12, 15] Different kinds of ligands have been described that are readily substituted, including NH_3,[16] nitriles,[17, 18] thioethers,[19, 20] or sulfonate.[21] These ligands are usually much easier to photodissociate than pyridines or imidazoles (see Chapter 2 of this thesis), because the energy gap between the ^{3}MLCT and ^{3}MC state are lower for complexes bound to these ligands.[22]

Usually, key factors proposed for the development of new PACT compounds are a suitable light activation window,[23] high photosubstitution efficiency,[24] and very different cytotoxicities between dark and light conditions.[15] When considering clinical applications, however, an anticancer drug should also have high solubility in aqueous solutions, good cellular uptake,

good stability in biological media, and excellent tumor selectivity.[25] In one word, the prodrug should be as biocompatible as possible. To improve biocompatibility, biological molecules such as peptides,[26 27] or proteins[28] can be attached to a (pro)drug. Most specifically, peptides are highly promising because of their biological activity, tuneable toxicity, and easy synthesis.[29, 30] On the other hand, peptides may be hydrolyzed *in vivo* by enzymes present in the blood stream, which can lower the efficacy and bioavailability of peptide-drug conjugates. To increase the metabolic and circulation half-life of peptides and peptide conjugates, different strategies have been described focusing on specific modifications at critical cleavage sites, including N-/C-terminal protection,[31] peptide cyclization,[32] the use of amide bond mimetics (e.g., thioamides, peptoids or β-amino acids),[33-35] or replacing natural L-amino acids by unnatural D-amino acids.[36] In general, most natural proteins and peptides are composed of L-amino acids; the complementarity between the L chirality of a peptide and that of its protein target often plays an important role in their stereospecific binding. This complementarity plays a role for both the targeted protein on the cancer cell surface, and for digesting enzymes.[37] Thus, a higher physiological stability is often found for peptides that contain D-amino acids, compared to L-peptide analogues that are readily digested by proteinases.[38, 39] On the other hand, the binding specificity of D-peptides to their protein target, essential for the active tumor targeting of anticancer drugs, as well as the potential side effects brought by D-amino acids, remain important questions in drug design.[40]

In Chapter 4, we reported that when a integrin targeted ruthenium-peptide conjugate $[Ru(Ph_2phen)_2(Ac\text{-}X_1RGDX_2\text{-}NH_2)]Cl_2$ contained one or two ruthenium-methionine bonds, its light-activation mechanism was closer to PACT than to PDT. In this work, we decided to explore the influence of amino-acid chirality on the (photo)chemistry and (photo)biology of $[Ru(Ph_2phen)_2(Ac\text{-}MRGDM\text{-}NH_2)]Cl_2$ complexes. Three peptide sequences were considered that either contained only L-amino acids (Ac-MRGDM-NH_2, called p1), only D-amino acids (Ac-mrGdm-NH_2, p2), or a mixture of L and D-amino acids (Ac-MrGdM-NH_2, p3).[c] In this chapter, M, R and D represent L amino acids and m, r, d are D-amino acids. These three peptides were coordinated to ruthenium(II) centers to generate a series of cyclic Ru-peptide conjugates, which were purified and fully analyzed in terms of structure, photochemistry, and biological properties *in vitro* (Scheme 5.1).

[c] Glycine(G) is excepted because it doesn't have a chiral center.

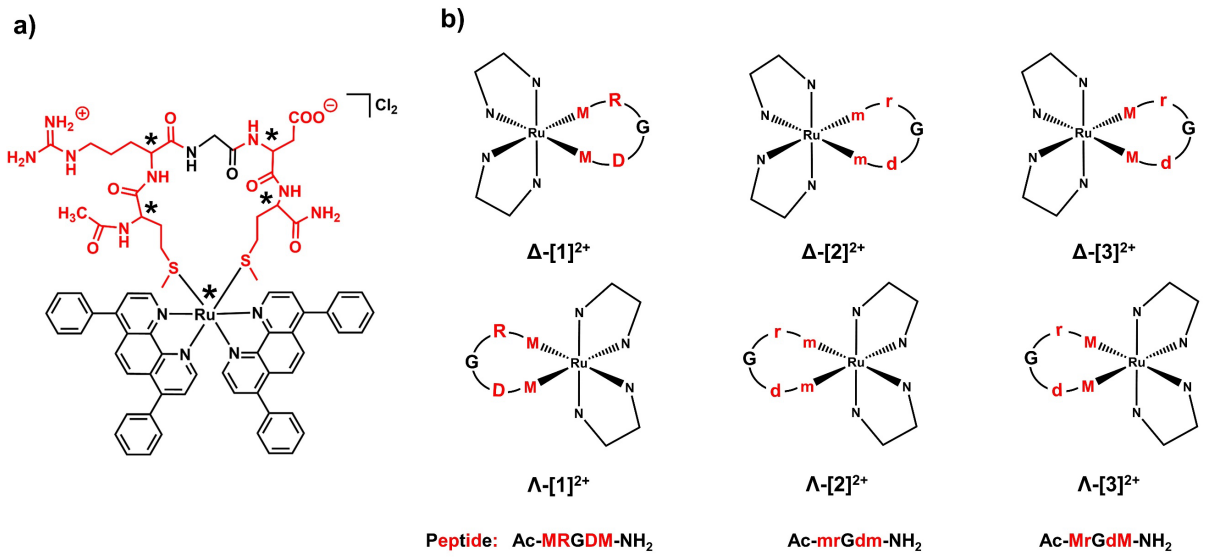

Scheme 5.1. *(a) General structure of the ruthenium-peptide conjugates prepared and analyzed in this chapter. The chiral center of the amino acids is labelled with asterisks. (b) Simplified structures of Δ-[**1**]$^{2+}$, Λ-[**1**]$^{2+}$, Δ-[**2**]$^{2+}$, Λ-[**2**]$^{2+}$, Δ-[**3**]$^{2+}$ and Λ-[**3**]$^{2+}$ formed from different combination of Δ-/Λ-isomers on the octahedral ruthenium center, and the peptides Ac-MRGDM-NH$_2$ (p1), Ac-mrGdm-NH$_2$ (p2) or Ac-MrgdM-NH$_2$ (p3). First column: Δ- and Λ-isomers of [**1**]$^{2+}$ carrying a fully L peptide. Second column: Δ- and Λ- isomers of [**2**]$^{2+}$ carrying a fully D peptide. Third column: Δ- and Λ- isomers of [**3**]$^{2+}$ carrying a mixed L/D peptide. Charges and terminal protecting group of the peptides are omitted for clarity.*

5.2 Results

5.2.1 Synthesis and characterization

Three ruthenium-peptide conjugates were synthesized from the three peptides and *rac*-[Ru(Ph$_2$phen)$_2$Cl$_2$], as reported in Chapter 4. Before coordination to Ru, p1 and p2 showed mirror CD spectra but identical proton nuclear magnetic resonance (^{1}H-NMR) spectra confirming they are enantiomers (Figure AV.1). Circular dichroism (CD) spectra of the three diastereomeric peptides showed a main peak around 228 nm with identical but either negative (p1) or positive (p2 & p3) ellipticity (Figure AV.2a), originating from n→π* transitions in the amide bonds.[41]

As a result of the octahedral Ru center bound to three bidentate chelating ligands, the Ru-p1, Ru-p2 and Ru-p3 conjugates have two diastereoisomers caused by the Δ or Λ configuration of the metal center in combination with the chirality of the L, D, or L/D peptide. All six diastereoisomers were isolated using high-performance liquid chromatography (HPLC, Figure 5.1a). Mass spectra (MS) analysis confirmed that the Ru:Ph$_2$phen:peptide ratio was 1:2:1

without any other ligand involved, implying the formula of ***[Ru(Ph$_2$phen)$_2$(peptide)]***$^{2+}$ in all six diastereomers (Figure AV.3). The 1D and 2D (COSY, NOESY and HSQC) NMR spectra reveal that upon coordination the thioether methyl peaks of the peptides (*e.g.*, δ = 2.10 ppm in p2) shifted upfield (*e.g.*, δ = 1.79 (N-terminal) /1.64 (C-terminal) ppm in Δ-[**2**]Cl_2) (Figure AV.1 *vs.* Figure AV.7). This observation, together with the mass analysis, proved that the two methionine residues were successfully coordinated to ruthenium, and hence that the conjugates were cyclic.

The Δ/Λ conformation of the complexes were then determined with CD spectroscopy. The configuration of the ruthenium center could clearly be established: Δ isomers of octahedral Ru(II) complexes are known to be characterized by a positive band at 270 nm and a deep negative ellipticity at 287 nm, while Λ isomers have opposite ellipticities at these wavelengths (Figure 5.1b).[42, 43, 44] The region between 200 and 230 nm would be characteristic for the peptide geometry. Upon coordination to Ru(II), the amide bond signals of peptides in CD spectra were basically lost (Figure AV.2a *vs.* b-d), thus the distinction of the spatial configuration of the peptides in [**1**]Cl_2–[**3**]Cl_2 was not feasible. Overall, for the six diastereomers the mirrored CD signals proved that the two HPLC-separated compounds were of opposite chirality (Δ/Λ).

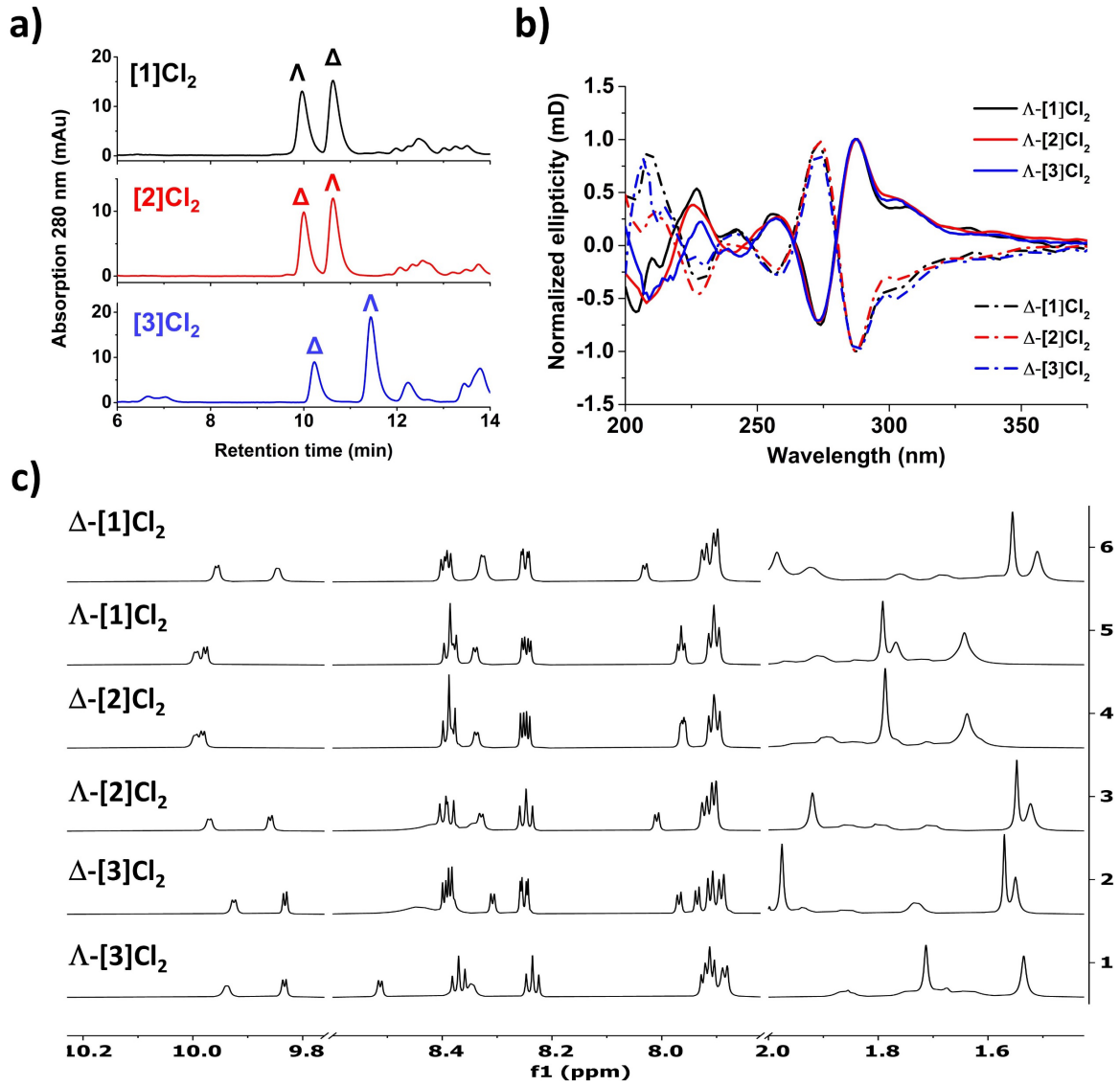

Figure 5.1. *(a) HPLC traces of the crude Ru-peptide conjugates [**1**]Cl_2, [**2**]Cl_2 and [**3**]Cl_2. Λ-/Δ-peaks are attributed according to Figure AV.2. Gradient: 30-40% acetonitrile/H_2O, 15 min, flow rate = 14 mL/min, collection UV channel = 280 nm. (b) Normalized CD spectra (0.1 mM, MilliQ H_2O) and (c) partial ^{1}H NMR spectra (850 MHz, CD_3OD) of HPLC-isolated Δ-[**1**]Cl_2, Λ-[**1**]Cl_2, Δ-[**2**]Cl_2, Λ-[**2**]Cl_2, Δ-[**3**]Cl_2 and Λ-[**3**]Cl_2. HPLC traces of the isolated samples are shown in Figure AV.4.*

Different Δ/Λ diastereomeric ratios were obtained for the three Ru-peptide conjugates, as shown in Figure 5.1a and Table 5.1. For [**1**]Cl_2, the Λ-isomer eluted first and the ratio of isomers was 1:1 according to HPLC peak integrals and synthetic yields. For [**2**]Cl_2 the ratio between the two isomers was also around 1:1, but the Δ isomer eluted first from the HPLC. These results are logical: the similar fraction ratio of Δ/Λ isomers from [**1**]Cl_2 and [**2**]Cl_2 is consistent with an identical racemic *cis*-[$Ru(Ph_2phen)_2Cl_2$] precursor and mirror-image peptides p1 and p2. For [**3**]Cl_2, the Λ isomer eluted at a much later retention time, and a 1:2 ratio of Δ-[**3**]Cl_2 and Λ-

[**3**]Cl_2 was observed, showing that changing the L-Arg and L-Asp residues in p1 to D analogues in p3 made the Λ configuration of the ruthenium complexes dominant (Table 5.1).

After full characterization, interesting structure correlation between the six diastereomers can thus be addressed. The compounds Δ-[**1**]Cl_2 and Λ-[**2**]Cl_2, as well as Δ-[**2**]Cl_2 and Λ-[**1**]Cl_2 were shown to be enantiomers by their mirrored CD spectra and identical NMR spectra (Figure 5.1b, 5.1c), due to the opposite chirality of the peptides p1 and p2:. This enantiomeric relationship was also confirmed by their identical retention times (Figure 5.1a and Table 5.1). For the pairs of diastereoisomers, the CD peaks were *almost* opposite due to the dominant ruthenium-based transitions, but not exact due to the contribution of the peptide. The differences were also clear from their non-identical NMR and retention times. (Figure 5.1).

Table 1. *Retention times, wavelength of the main CD peaks, and integral HPLC area ratio of Λ/Δ isomer in [**1**]Cl_2, [**1**]Cl_2 and [**3**]Cl_2 (amount of Δ-isomer is defined to be 1).*

Complex	R_T (min)	Main Band in CD	Ratio to corresponding Δ-isomer
Δ-[**1**]Cl_2	10.6	+274 nm / -287 nm	1
Λ-[**1**]Cl_2	9.96	-274 nm / +287 nm	1
Δ-[**2**]Cl_2	10.0	+274 nm / -287 nm	1
Λ-[**2**]Cl_2	10.6	-274 nm / +287 nm	1.1
Δ-[**3**]Cl_2	10.2	+274 nm / -287 nm	1
Λ-[**3**]Cl_2	11.4	-274 nm / +287 nm	2

5.2.2 Photochemistry studies

A prodrug candidate for PACT should be not only photoactive but also thermally stable when kept in the dark, which can be monitored with UV-vis spectroscopy (Figure AV.15). The absorption spectra of the six compounds in water are comparable, as all six complexes show a single broad absorption band in the visible region between 400 and 500 nm, with an absorption maximum located around 405 nm (Figure 5.2 and Figure AV.16). The molar extinction coefficients (ε_{max} at 405 nm) of [**1**]Cl_2–[**3**]Cl_2 in water are very also similar (Table 5.2). The thermal stability of the six complexes was tested in MilliQ H_2O and cell culture medium by monitoring their UV-vis spectra in the dark over time. No changes were observed for at least 60 h in water and 100 h in cell culture medium (see representative dataset for Δ-[**2**]Cl_2 in Figure AV.15), showing that the complexes are thermally stable in these conditions.

To determine the potential of the six isomers as PACT prodrugs, the time evolution of their absorbance spectra was monitored under green light activation (515 nm, ± 4 mW/cm^2) in two solutions, *i.e.,* H_2O or 1:1 v/v H_2O:MeCN. Representative spectra for the photosubstitution reaction of Δ-[**1**]Cl_2 are presented in Figure 5.2. The spectra for the other five isomers are shown in Figure AV.16. A redshift of the broad absorbance peak was observed upon irradiation of the compound in pure H_2O. The mass spectra after irradiation showed the presence of the bis-aqua photoproduct $[Ru(Ph_2phen)_2(H_2O)_2]^{2+}$ (found 268.2, calcd *m/z* 267.7 for $[M + H]^{3+}$, Figure AV.20a). Irradiation of solutions containing acetonitrile resulted in an increase of the absorbance of the broad peak, with barely any shift of the absorption maximum, and a much faster photoreaction seemed to occur (inset in Figure 5.2b). Mass spectra after light irradiation in 1:1 v/v H_2O:MeCN showed the photoproduct to be $[Ru(Ph_2phen)_2(CH_3CN)_2]^{2+}$ (found 424.1, calcd *m/z* 424.1, Figure AV.20b). The released peptide Ac-MRGDM-NH_2 was also detected by MS at 650.4 (calcd. *m/z* 650.3 for $[M + H]^+$) in both conditions. The five other diastereomers showed similar evolution of their absorbance spectra. Overall, all six isomers can be photoactivated with green light and release the peptide through substitution by H_2O or acetonitrile ligands from the solvent.

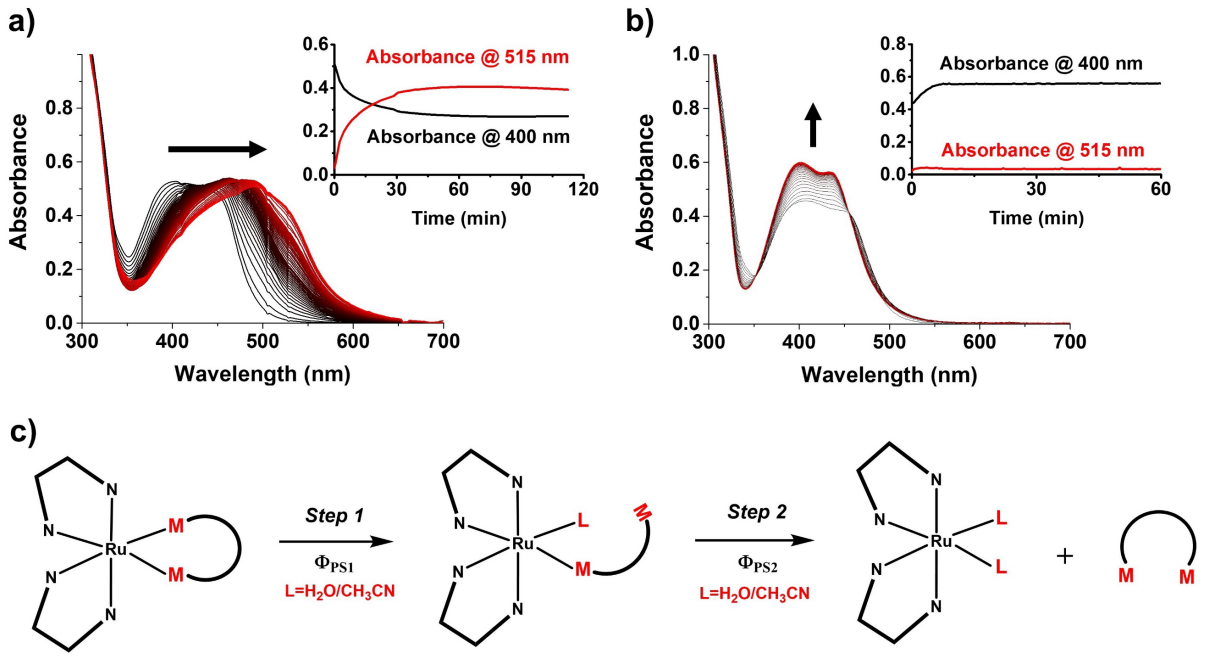

Figure 5.2. *Time evolution of the absorbance spectrum of* ***Δ-[1]***$^{2+}$ *(50 μM) in H_2O (a) and 1:1 v/v H_2O:CH_3CN (b) during 120 min irradiation with a 4 mW/cm^2 515 nm light source. Inset: time evolution of the absorbance at 400 nm or 515 nm vs. irradiation time. c) Simplified scheme of the two-step photosubstitution process when Ru-peptide conjugate was irradiated with green light in either H_2O (L=H_2O) or H_2O/MeCN mixture (L=CH_3CN), p1, p2 and p3 are simplified by M-M.*

The efficiency of photosubstitution in [**1**]Cl_2–[**3**]Cl_2 was quantified both in H_2O and in H_2O/MeCN mixture by calculating the individual photosubstitution quantum yields $\mathbf{\Phi_{PS1}}$ and $\mathbf{\Phi_{PS2}}$ for each step of the two-step peptide photosubstitution reaction (Table 5.2 and Figure AV.17-19). Peptide dissociation is a two-step photoreaction (see Chapter 4), where the first methionine is substituted by one solvent molecule upon absorption of a first photon, after which the second methionine may be photosubstituted upon absorption of a second photon, with lower quantum yield $\mathbf{\Phi_{PS2}}$ (Figure 5.2c). In principle, good PACT compounds should have reasonable (>0.001) photosubstitution quantum yields. On average, the $\mathbf{\Phi_{PS1}}$ values were higher than the $\mathbf{\Phi_{PS2}}$ values in both conditions. $\mathbf{\Phi_{PS1}}$ in H_2O was high (>0.1) and quite similar in 1:1 v/v H_2O:CH_3CN. The fact that the first methionine dissociation is quite fast even in presence of comparatively weak ligands such as H_2O, suggesting these ruthenium-peptide cyclic conjugates can be efficiently activated by light. For the second step, however, photosubstitution by CH_3CN was found to be up to one order of magnitude more efficient than photosubstitution by H_2O, which suggests that once the strain of the cycle has been released, the nature of the incoming ligand plays an important role on the rate of photosubstitution.[45, 46] Comparable $\mathbf{\Phi_{PS1}}$ and $\mathbf{\Phi_{PS2}}$ values were found for the six diastereomers, although in presence of MeCN the two isomers of [**3**]Cl_2 were the most labile compounds for both photosubstitution steps (Δ or Λ: $\mathbf{\Phi_{PS1}}$=0.20 or 0.21 and $\mathbf{\Phi_{PS2}}$=0.0067 or 0.0072, respectively).

Considering the essentially similar photosubstitution behavior and the results of Chapter 4, we expected that the series of Ru-peptide conjugates are PACT rather than PDT compounds. As an evaluation of the efficiency of these compounds as PDT type II agents, the quantum yields ($\mathbf{\Phi_{\Delta}}$) of singlet oxygen ($^1O_2$) generation were further measured for [**1**]Cl_2–[**3**]Cl_2 in air-saturated CD_3OD (Figure AV.21 and Table 5.2). The $\mathbf{\Phi_{\Delta}}$ value for the mixture of Δ- and Λ- isomers of [**1**]Cl_2 was already reported in Chapter 4 (0.013 ± 0.005); within experimental errors the values found for the isolated isomers were identical and very low (0.008 ± 0.005 and 0.009 ± 0.005). Overall, the $\mathbf{\Phi_{\Delta}}$ of all six isomers were quite similar and lower than 0.015, indicating that these compounds are not likely to be good sensitizers for PDT type II. In conclusion, from our photochemical studies all diastereomers of [**1**]Cl_2–[**3**]Cl_2 are able upon light activation to open their cycle with high efficiency and release their peptide with lower efficiency *via* a two-step photosubstitution reaction. At the same time they were shown to be weak $^1O_2$ generators, predicting them to be potential prodrugs for PACT.

Table 5.2. *Photochemical properties of isolated* Δ and Λ *diastereoisomers of [**1**]Cl_2–[**3**]Cl_2 including molar extinction coefficients (ε, in M^{-1} cm^{-1}) at absorption maximum wavelength (405 nm), photosubstitution quantum yields for step 1 (Φ_{PS1}) and step 2 (Φ_{PS2}) in H_2O or 50% MeCN in H_2O, and singlet oxygen quantum yields of each complexes in CD_3OD.*[a]

Complex	$\varepsilon \times 10^4$ (M^{-1} cm^{-1}) at 405 nm	Φ_{PS1} in H_2O	Φ_{PS2} in H_2O	Φ_{PS1} in 1:1 H_2O: CH_3CN	Φ_{PS2} in 1:1 H_2O: CH_3CN	Φ_{Δ} ($^1O_2$)
Δ-[**1**]Cl_2	1.21	0.15	0.0059	0.17	0.043	0.008
Λ-[**1**]Cl_2	1.18	0.19	0.0057	0.14	0.030	0.009
Δ-[**2**]Cl_2	1.16	0.26	0.0052	0.11	0.032	0.009
Λ-[**2**]Cl_2	1.27	0.22	0.0050	0.17	0.057	0.014
Δ-[**3**]Cl_2	1.05	0.17	0.0092	0.21	0.067	0.011
Λ-[**3**]Cl_2	1.12	0.15	0.0073	0.20	0.072	0.005

[a] *For $^1O_2$ measurements $[Ru(bpy)_3]Cl_2$ was used as a reference compound, with $\Phi_{\Delta} = 0.73 \pm 0.12$ in air-saturated CD_3OD.*[47]

5.2.3 Integrin expression and cellular uptake

The ruthenium-peptide conjugates are intended to target specifically integrin proteins (see Chapter 1 and Chapter 4), thus for the biological studies two human cancer cell lines were chosen that were reported to have different integrin expressions levels: A549 (human adenocarcinoma alveolar basal epithelial cells) and PC-3 (human prostate cancer cells). The expression levels of the two integrin heterodimers $\alpha_v\beta_3$ and $\alpha_v\beta_5$ in both cell lines were first compared using a reported double-immunofluorescence protocol.[48] As discussed in Chapter 3, besides the differences in integrin expression between different cell types, it has also been reported that the integrin protein family can be up-regulated by HIF activation in a cell subjected to O_2 shortage.[49-51] Thus, cells cultured in normoxic (21% O_2) or hypoxic incubators (1% O_2) were included in the assay. The integrin expression levels of all cell lines quantified by mean relative florescent intensities are summarized in Figure 5.3a; the corresponding histograms are shown in Figure AV.22. For integrin $\alpha_v\beta_3$, the difference in expression between A549 and PC-3 was quite limited; however, A549 was found to have significantly higher expression for $\alpha_v\beta_5$ than PC-3 in normoxic conditions. Interestingly, for PC-3 and A549 higher expression of $\alpha_v\beta_3$ was observed in hypoxia than in normoxia, but the difference was not

significant for integrin $\alpha_v\beta_5$. The observed up-regulation of the $\alpha_v\beta_3$ integrin could make it a possible target for the treatment of hypoxic regions of tumors with [**1**]Cl_2–[**3**]Cl_2.[52, 53]

The cellular uptake of the different diastereomers in the two cell lines and in two dioxygen concentrations was investigated. The amount of ruthenium in a cell can be measured with inductively coupled plasma mass spectrometry (ICP-MS), as there is no ruthenium in a normal cell. A549 and PC-3 cells in either normoxia or hypoxia were incubated for 24 h with [**1**]Cl_2–[**3**]Cl_2 (10 μM), then washed with ruthenium-free medium, and finally digested with acid to determine intracellular ruthenium concentrations with ICP-MS. The uptake results quantified as μg Ru/million cells are shown in Figure 5.3b. The differences in uptake between A549 and PC-3 cells as well between the six diastereomers were quite small in normoxia. However, the cellular uptake in hypoxic cells increased significantly for A549, as well as for PC-3 cells although at a smaller level. These observations fit better with the relative expression levels of integrin $\alpha_v\beta_3$ in normoxic and hypoxic cells, than with the expression levels of $\alpha_v\beta_5$. On the other hand, ruthenium accumulation was higher in hypoxic A549 cells than in hypoxic PC-3 cells; considering the non-significant difference in $\alpha_v\beta_3$ expression between hypoxic A549 and PC-3 cells, other integrin heterodimers may be involved in the binding and uptake of the RGD-functionalized anticancer drugs.[54] When comparing the different compounds, the Ru-peptide conjugates with D-amino acids, [**2**]Cl_2, were taken up in slightly lower amounts than [**1**]Cl_2, suggesting that [**2**]Cl_2 may interact less strongly with the $\alpha_v\beta_3$ receptor. Overall, the highest uptake efficiency was found in hypoxic A549 cells, which is consistent with the high integrin expression observed in this cell line.

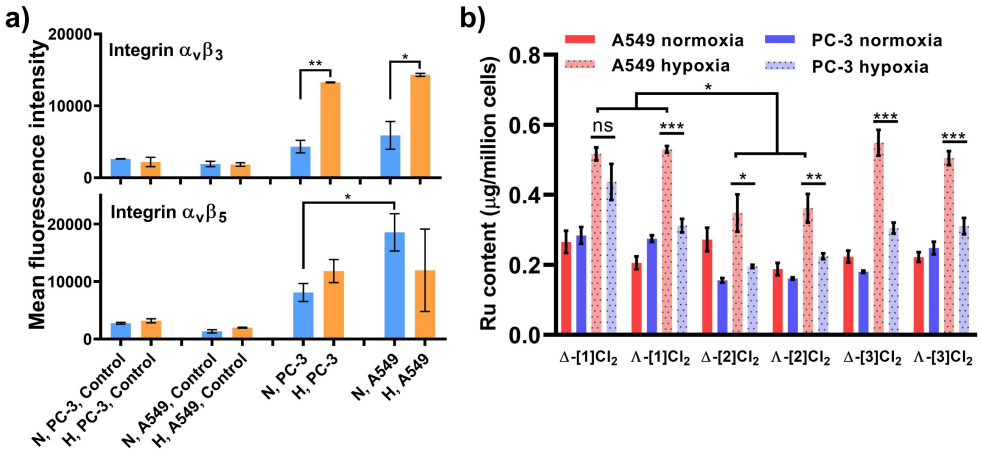

Figure 5.3. *(a) Expression of integrin $\alpha_V\beta_3$ and $\alpha_V\beta_5$ in A549 and PC-3 human cancer cell lines under normoxic (21% O_2, blue bars) or hypoxic (1% O_2, orange bars) conditions. Y-axis (N: normoxia, H: hypoxia) shows the fluorescence intensity of cells incubated with either anti-integrin $\alpha_V\beta_3$ or anti-integrin $\alpha_V\beta_5$ primary monoclonal antibodies, followed by secondary antibody conjugated to Alexa-*

*Fluor 488. Control indicates cells that were incubated with secondary antibody only and hence should not be emissive. Error bars show standard deviations (SD) from duplicate (n=2) experiments. (b) Ru content (μg Ru/million cells) of normoxic and hypoxic A549 and PC-3 cells incubated with one of the six diastereomers of [**1**]Cl_2–[**3**]Cl_2 (10 μM, 24 h), as determined by ICP-MS. Error bars indicate standard deviation from six experiments. Unpaired t-test was used to determine the significance of the comparisons of data (*P < 0.05; **P < 0.01; ***P < 0.001; ****P < 0.0001).*

5.2.4 Anticancer study in 2D cell monolayers and 3D tumor spheroids

Considering the potential of the six diastereomers as PACT complexes, their cytotoxicity was determined for 2D monolayers of A549 cells using a sulforhodamine B (SRB) cell quantification end point assay,[55] in the dark (light dose 0 J/cm^2) or upon green light activation (light dose 13.1 J/cm^2), both in normoxic and hypoxic conditions. Half-maximal effective concentrations (EC_{50} in μM) were measured as an evaluation of the toxicity of the compounds. The photoindex values (PI), defined as $EC_{50,dark}$/ $EC_{50,light}$, were calculated to quantify the extent of light activation in cancer cells. The dose-response curves and the corresponding EC_{50} values are shown in Figure AV.23-26 and Table 5.3, respectively. In a first approach, to prove that the Ru-RGD conjugates were photoactivated, A549 cells were treated with purified Δ or Λ isomers of [**1**]Cl_2–[**3**]Cl_2 (24 h), and activated by light without refreshing the medium before light activation. In such a protocol, compounds that did not bind to the integrin target remain in solution after light activation, which maximizes their chances to be taken up and to kill the cells *after* light activation, *i.e.,* irrespective of their integrin-binding properties. $EC_{50,light}$ values in normoxic A549 cells were between 1.9 and 3.0 μM for the six diastereomers, resulting in promising PI values between 11 and 17. In hypoxic A549 cells, the $EC_{50,light}$ increased by a factor 2 (5.0-7.0 μM), which was expected because hypoxic cells are often found more resistant to chemotherapy, which should lead to increased EC_{50} values in both dark and light conditions. However, as the $EC_{50,dark}$ values became lower than those in normoxia, the PI values in hypoxia were reduced to 3.0-4.5, *i.e.,* by a factor ~4 compared to normoxia. The lower $EC_{50,dark}$ values observed under hypoxia were unexpected; possibly this may be explained by the higher cellular uptake of the complexes (Figure 5.3b), resulting from the up-regulation of integrins in hypoxia. On the other hand, increased integrin expression should also lead to increased toxicity *after* light activation, which we did not observe. A hypothesis for this result may be that hypoxic cells are more resistant to the photoproduct of the conjugates (*i.e.* $[Ru(Ph_2phen)_2(H_2O)_2]^{2+}$) than to non-activated conjugates, which cause cell death in the dark. Overall, this series of diastereomers showed promising PACT properties in both normoxic and hypoxic conditions,

but the absence of a washing step before light activation made proper analysis of the cytotoxicity data complicated.

Table 5.3. *Half-maximal effective concentrations (EC_{50} in μM) with 95% confidence intervals (±CI in μM) and photoindexes (PI) for* ***[1]***Cl_2*–*** ***[3]***Cl_2 *in the dark or upon green light irradiation, in 2D monolayers of A549 or PC-3 cell lines and in 3D A549 tumor spheroids grown under normoxic condition.* [a, b]

Cell line	Condition	Light Dose J/cm²	Δ-[1]Cl_2			Λ-[1]Cl_2			Δ-[2]Cl_2			Λ-[2]Cl_2			Δ-[3]Cl_2			Λ-[3]Cl_2		
			EC_{50} (μM)	±CI	**PI**	EC_{50} (μM)	±CI	PI	EC_{50} (μM)	±CI	**PI**	EC_{50} (μM)	±CI	**PI**	EC_{50} (μM)	±CI	**PI**	EC_{50} (μM)	±CI	**PI**
A549	Normoxia *no wash*	0	33	+17 -9.9	**12**	49	+35 -10	**16**	27	+9.9 -7.1	**11**	31	+8.6 -6.3	**12**	32[c]	+13 -8.7	**17**	49	+39 -10	**16**
		13.1	2.7	+0.9 -0.7		3.0	+0.8 -0.7		2.4	+0.8 -0.7		2.5	+0.84 -0.71		1.9[c]	+0.9 -0.7		3.0	+1.2 -0.97	
	Hypoxia *no wash*	0	21.1	-4.1	**3.7**	18.3	-3.9	**3.0**	23.6		**4.5**	29.4	+8.6	**4.4**	n.d. [d]			24.6		**4.0**
		13.1	5.7	+0.6 -0.5		6.0	+0.9 -0.7		5.3	+0.3 -0.3		6.7	+0.7 -0.6					6.2	+0.7 0.6	
	Normoxia *wash*	0	>50		**>3.8**	>50		**>6.3**	>50		**>6.9**	>50		**>5.1**	36	+16 -9.2	**7.2**	21	-2.3	**7.8**
		13.1	13	+2.3 -1.9		8.0	+2.8 -2.2		7.2	+1.5 -1.2		9.9	+2 -1.6		5.0	+2.6 -2.1		2.7	+0.4 -0.4	
	Hypoxia *wash*	0	>50		**>1.6**	>50		**>1.3**	>50		**>3.1**	>50		**>1.9**	31	+3 -2.9	**2.2**	25	+5.7 -5.3	**3.3**
		13.1	31	+6.9 -6.3		34	+22 -11.7		16	+3.2 -2.7		27	+14 -8.1		14	+3.7		7.5	+1.1 -1	
A549 spheroids		0	>100	-	**>5**	>100	-	**>4**	>100	-	**>3**	>100	-	**>5**	n.d. [d]					
		13.1	17	4.5 -3.6		23	4.8 -3.9		27	5.9 -4.8		18	3.4 -2.9							

[a] *PI =* $EC_{50,\ dark}/EC_{50,\ light}$. [b] *Irradiation condition: normoxia 520 nm, 10.9 mW/cm², 13.1 J/cm², 20 min; hypoxia 520 nm, 7.22 mW/cm², 13.1 J/cm², 30 min.* [c] *n=2 instead of n=3 due to limited compound stock.* [d] *n.d. = not determined, Drugs* ***[3]***Cl_2 *were not included in this study due to insufficient reserve of these compounds. The medium was not refreshed to prevent disintegration of the spheroids.*

To better compare the targeting performance of the different diastereomers, a washing step was introduced just before light irradiation. This additional step should allow to relate cell death to the uptake efficiency of compounds in the cells, or their stronger binding to integrin before light irradiation. The cytotoxicity data obtained with this new protocol are shown in Table 5.3, and the corresponding data are summarized in Figure 5.4. Among the six diastereomers, differences between [**1**]Cl_2 and [**2**]Cl_2 were not significant. However, Λ-[**3**]Cl_2 clearly showed the highest toxicity (EC_{50}) both in the dark and after light activation, and both in hypoxia and normoxia. It seems that the cellular uptake is not significantly changed upon replacement of Ac-MRGDM-NH_2 by Ac-MrGd-M-NH_2 (Figure 5.3b), but the toxicity to A549 cancer cells does increase significantly. The chirality of the peptide hence seems to influence the biological properties of the PACT ruthenium compound.

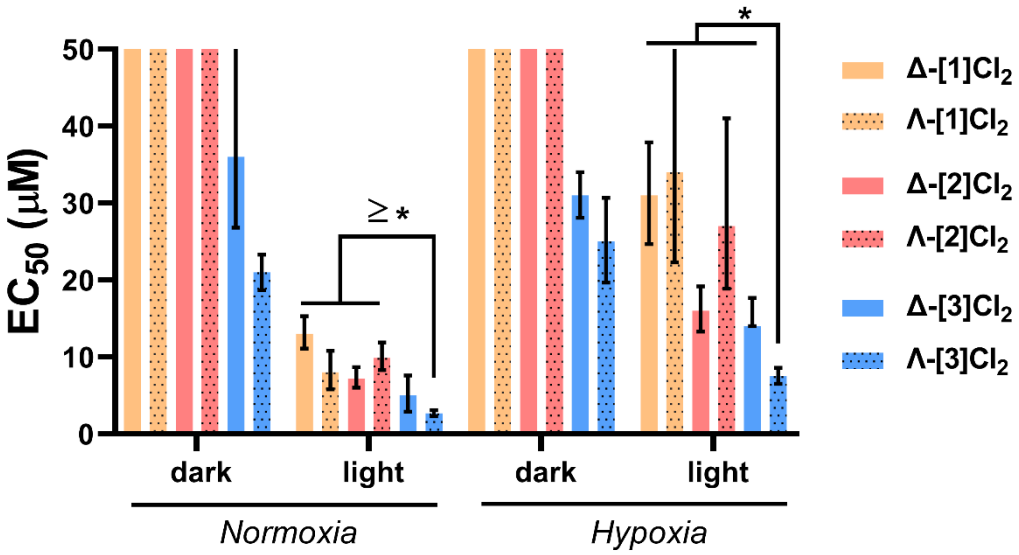

Figure 5.4. *EC_{50} values in 2D monolayers of A549 human lung cancer cell lines upon treatment with isolated isomers of [**1**]Cl_2–[**3**]Cl_2 in normoxia (37 °C, 21% O_2) or hypoxia (37 °C, 1% O_2) in a protocol* ***that includes a washing step*** *(medium replacement by drug-free medium) before light activation. Irradiation was performed 24 h after prodrug addition. Irradiation conditions: in normoxia 520 nm, 10.9 mW/cm², 20 min, 13.1 J/cm²; in hypoxia 520 nm, 7.22 mW/cm², 30 min, 13.1 J/cm². Bars out of range represent EC_{50} values above 50 μM. The exact values are shown in Table 5.3 and errors were 95% confidence intervals (±CI in μM). Unpaired t-test was used to determine the significance of the comparisons of data (*P < 0.05; **P < 0.01; ***P < 0.001; ****P < 0.0001).*

A three-dimensional (3D) tumor spheroids model (A549) was further used to assess the efficacy of these ruthenium-peptide conjugates, to better simulate the biological environment of physiological tumors. Compared to 2D cell layers, 3D spheroids form a better model for the penetration of the prodrug, of light, and of dioxygen into the tumor.[56] The treatment protocol

was similar to the first protocol used in 2D; however, to avoid disturbing the physical structure of the spheroids, washing with Ru-free media was not applied before irradiation. The EC_{50} values were determined by an ATP quantification end point assay called Cell Titer Glo 3D (Table 5.3, Figure AV.28). In parallel, the morphology of the A549 spheroids were captured by bright field microscopy (Figure AV.27). The $EC_{50,dark}$ values were all higher than 100 μM, which is more than two times higher than those observed in normoxic A549 2D monolayers. Importantly, the relatively high PI values observed in 2D were retained in 3D (PI>5). In fact, the $EC_{50,light}$ values were found to be between 17 and 27 μM, which is 5-10 times higher than those measured in A549 monolayers. This difference is significant, notably when compared with the cisplatin control, which showed a EC_{50} (3.3 μM) in 3D that is close to that measured in 2D A549 monolayers (~ 2.3 μM, Chapter 3, Table 3.1). The photoproduct $[Ru(Ph_2phen)_2(H_2O)_2]^{2+}$ of the PACT compounds possibly penetrated less easily into the spheroids, compared to cisplatin. Moreover, the spheroid size in our experiments was larger than usual because of the high number of seeding cells and late treatment (diameter in capture day >1000 μm, seeding-to-treatment time: 4 days compared to 3 days in Chapter 3 and 4), which decreased the EC_{50} values of the drugs in both dark and light conditions. Still, the $EC_{50,dark}$ values of **[1]**Cl_2-**[2]**Cl_2 were found to be higher than 100 μM, further confirming the low toxicity of the ruthenium PACT prodrugs before light activation. Spheroids with a diameter >400 μm can already develop a hypoxic core, in which the hypoxia-signaling pathway is also activated.[57] The promising photoactivated toxicity of the six diastereomers in the large-sized spheroids (with PI up to >5), predict them to have high potential as PACT complexes *in vivo*.

To determine the pathway by which the compounds cause cell death, a ROS generation assay was performed using the unspecific molecular probe CellROX™ Deep Red. This assay was used to quantify the formation of singlet oxygen, superoxide, and hydroxide radicals, by Δ and Λ isomers of complexes [**1**]Cl_2–[**3**]Cl_2 in A549 cells, both in the dark or upon green light irradiation (515 nm, 13.1 J/cm^2). *Tert*-butyl hydroperoxide (tBHP), cisplatin and Rose Bengal were used as positive control, negative control, and green light-activated PDT type II control, respectively; the experiments were conducted both in normoxic and hypoxic cells. The mean florescence intensity in each cell is a measure for ROS production, which was quantified by flow cytometry (FACS) and normalized to that of controls (see Table 5.4 and raw data in Figure AV.29 and 30). In the end of the assay, the absolute ratio R, defined as the ratio of the ROS probe emission intensity in the light group, divided by that in the dark group, was used as quantification of light-induced ROS production.

When cells were cultured with any of the six ruthenium complexes and left in the dark, ROS generation was not observed (R = 0.57-1.24). When light was applied in presence of a ruthenium complex, R values higher than 1 were observed in normoxia (R = 1.8-6.2); some of the compounds generated as much ROS as the PDT agent Rose Bengal (R = 5.2). Significant variations in ROS production were observed for the different isomers, from R=1.8 with Λ-[**2**]Cl_2, which is identical to the control with light only, to R = 6.2 for the enantiomer Δ-[**1**]Cl_2, which is higher than that of Rose Bengal. Overall, non-negligible amounts of ROS were generated by light irradiation of the prodrugs in normoxic conditions, consistent with the observations described in Chapter 4. We interpret this result as a consequence of the interaction of the bis-aqua photosubstitution product $[Ru(Ph_2Phen)_2(OH_2)_2]^{2+}$ with histidine residues in endogenous proteins, which may form ruthenium-histidine adducts capable of producing ROS, as discussed in Chapter 4. In hypoxia, however, the R values after light activation were found to be between 1.0 and 2.2, which is quite close to the negative control cisplatin. Thus, no significant ROS generation occurred with or without light activation at 1% O_2. In combination with the cytotoxicity study in hypoxia, we conclude that the phototoxicity of this series of Ru-peptide conjugates in hypoxia is not based on the generation of ROS, while in normoxia ROS generation plays a significant role in their phototoxicity.

Table 5.4. *Normalized intracellular ROS generation in A549 cells according to FACS analysis using CellROX™ Deep Red Reagent as probe, after treatment with Δ- or Λ-[**1**]Cl_2–[**3**]Cl_2, cisplatin, Rose bengal (15 μM, 24 h), in the dark and after light irradiation (515 nm, 13.1 J/cm²).*[a, b]

Complex	Normoxia (21%)			Hypoxia (1%)		
	dark	Light	R	dark	Light	R
tBHP	14.00			4.36		
Control	1.00	2.06	2.06	1.00	1.55	1.55
Δ-[**1**]Cl_2	0.63	3.88	6.18	0.78	1.04	1.32
Λ-[**1**]Cl_2	0.57	2.61	4.58	1.03	1.70	1.65
Δ-[**2**]Cl_2	1.10	4.80	4.37	1.12	1.18	1.04
Λ-[**2**]Cl_2	1.24	2.20	1.77	1.22	1.83	1.50
Δ-[**3**]Cl_2	1.01	2.97	2.95	1.07	1.92	1.78
Λ-[**3**]Cl_2	1.05	3.55	3.39	0.91	1.99	2.20
Cisplatin	1.28	2.23	1.74	1.00	1.99	2.00
Rose Bengal	0.90	4.71	5.21	0.84	2.56	3.05

[a] ROS amounts were quantified by normalized mean florescence intensity (Figure AV.29 and 30) to dark control (normoxia: 18194; hypoxia: 16637) in corresponding groups. [b] tBHP (250 μM, 1 h) was used as positive control for oxidative radical production.

5.3 Discussion

Replacement of Ac-MRGDM-NH_2 (peptide p1) by the fully D-peptide analogue Ac-mrGdm-NH_2 (p2) led to slightly lower uptake of the ruthenium prodrug in hypoxic A549 cells while the observed cytotoxicity appeared to be similar. Replacement of the L-Arg and L-Asp residues of p1 by D-Arg and D-Asp (p3) seemed to lead to more significant changes in the properties of the prodrug, as Λ-[**3**]Cl_2 showed the highest phototoxicity in A549 cells. Considering its similar cellular uptake, compared with [**1**]Cl_2, its 25-50% enhanced quantum yield of the second photosubstitution step could at least partly explain the higher toxicity to cells after light activation at a given light dose, if only a PACT mechanism is considered. This means that the high efficiency of the second step of the peptide being replaced by targeted biomolecules seems to be more critical. Yet, the behavior of all six isomers are qualitatively similar in terms of their photoactivation route (two-step photosubstitution followed by ROS production by the photoproduct). Overall, the efficacy of these Ru-peptide conjugates to large-sized tumor spheroids (>1000 μm) is promising, with PI values higher than 5. Considering the ROS production by the photoproducts in normoxia, it is highly possible that a dual action is responsible for this good response in tumor spheroids: on the edge of the spheroids, cells could be killed by both the $[Ru(Ph_2phen)_2(H_2O)_2]^{2+}$ photoproduct and ROS, with a synergistic PDT+PACT mechanism, while in the deeper core of the spheroids where PDT is no longer accessible, cells would mainly die via the sole action of $[Ru(Ph_2phen)_2(H_2O)_2]^{2+}$.

In spite of these promising observations, the story needs further investigations. First, as discussed in the introduction, a more relevant topic in the field is to know whether the presence of D-amino acids in peptides p2 and p3 results in higher stability in physiological conditions, *i.e.,* in presence of proteases. Proteolytic stability of these conjugates can be typically measured using HPLC or LC-MS after treatment with human plasma or blood sampling *in vitro*.[57] Ideally, after intravenous injection in a mice model, the retention time of these compounds in blood would need to be measured, as well as their tumor accumulation efficiency. Second, it needs to address whether replacement of L- by D-amino acids would decrease the conjugates' integrin binding affinities*:* protein interaction study (as described in Chapter 3) or docking simulation studies may allow to get the answer. If Λ-[**3**]Cl_2 would show enhanced stability in plasma while

keeping its integrin binding affinity, considering its properties highlighted in this work, it would could be the isomer of the series with the highest potential for clinical application.

5.4 Conclusion

Although several questions need to be addressed further, in this study six isomers of the $[Ru(Ph_2phen)_2(px)]^{2+}$ conjugate were synthesized, isolated, and characterized successfully. Structural relation of three pairs of stereoisomers, *i.e.,* Δ- and Λ-[**1**]Cl_2, [**2**]Cl_2 and [**3**]Cl_2, in between two pairs of enantiomers Δ-[**1**]Cl_2 *vs.* Λ-[**1**]Cl_2 and Λ-[**1**]Cl_2 *vs.* Δ-[**2**]Cl_2 are confirmed. A combination of physical, chemical, and biological studies suggested that the compounds behave as PACT complexes, including high photosubstitution quantum efficiencies, poor $^1O_2$ generation properties for the caged prodrug itself, and PI values that remain higher than 1 even in hypoxic conditions. Once activated by light in living cells, however, they generate photodynamically active species that contribute in normoxic cells to light-induced cell death. All in all, the use of D-amino acids in the peptide chain did not result in a decrease of the PACT efficiency of the Ru-peptide conjugates. Among the six diastereomers characterized, Λ-[**3**]Cl_2 was found to have the highest photosubstitution efficiency in H_2O/MeCN mixtures and also the highest *in vitro* cytotoxicity. Overall, we believe this work offers promising perspectives for the development of coordination complexes for PACT cancer treatment based on ruthenium and methionine-containing peptides.

5.5 Experimental section

5.5.1 General

The photochemistry studies by UV-vis, following photosubstitution quantum yields calculation, integrin expression, cytotoxicity assays (2D) and measurement of intracellular ROS were carried out according to the methods descriped in Appendix I.

5.5.2 Compounds preparation

The peptides were purchased from Biomatik or ChinaPeptides, and applied in synthesis without any further purification. *cis*-$[Ru(Ph_2phen)_2Cl_2]$ was synthesized according to an existing procedures.[10] The general synthesis procedure of Ru-peptide conjugates was as follows: *cis*-$[Ru(Ph_2phen)_2Cl_2]$ (0.10 mmol, 83.6 mg) was added to a 50 mL two-neck flask and purged with N_2 three times. The peptide p1, p2, or p3 (0.10 mmol, 65.0 mg) was dissolved in water (8 mL) and the pH adjusted to 7 by adding 1 M NaOH. After adding deoxygenated ethanol (8 mL) to the reaction flask, the peptide aqueous solution was deoxygenated by N_2 bubbling for 10 min

and injected into the reaction flask. The reaction mixture was then refluxed for 7 days at 80 °C under N_2. Then, ethanol was rotary evaporated, and the remaining aqueous mixture was filtered (RC 60 Membrane Filters, cytiva) under vacuum and washed with MilliQ water (~ 20 ml × 3 times). The combined filtrate was freeze-dried and stored until purification by high-performance liquid chromatography (HPLC).

The HPLC purification was realized on a 250 x 21.2 mm Jupiter® 4 µm Proteo 90 Å C12 column using the Thermo Scientific UHPLC system. The gradient was controlled by four pumps. The mobile phase consisted in water containing 0.1% v/v formic acid (phase A) and acetonitrile containing 0.1% v/v formic acid (phase B). The gradient for the preparative separation of [**1**]Cl_2 -[**3**]Cl_2 was 30−40% phase B/phase A for 15 min with a flow rate 14 mL/min. The fractions were monitored by four UV detector (set at 214 nm, 290 nm, 350 nm, and 450 nm) and collected based on the trace of the UV detector (290 nm). After purification, the Δ/Λ stereochemistry of each compound was assigned by CD measurements. The characterization details for the six diastereomers are shown below and in Appendix V.

[Ru(Ph$_2$phen)$_2$(Ac-MRGDM-NH$_2$)]Cl$_2$ ([1]Cl$_2$)

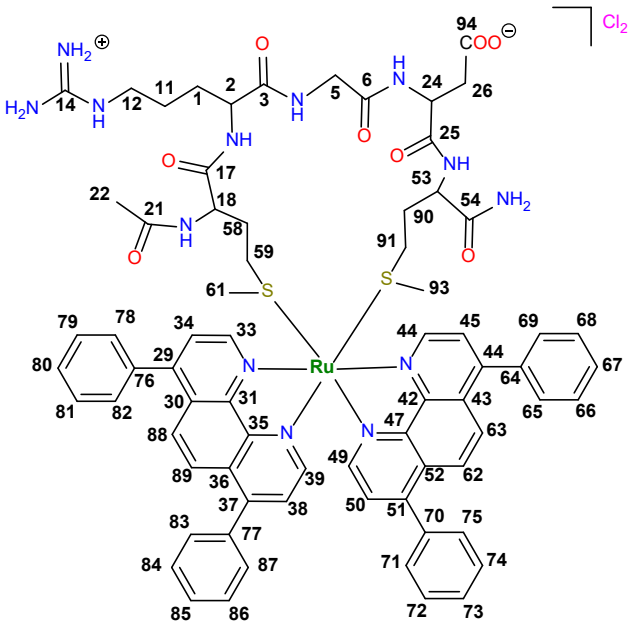

Δ-[1]Cl_2 (6.41 mg, 4.3 µmol, 5%). **HPLC** R_T: 10.6 min (during purification). ^{1}H NMR (850 MHz, δ in CD_3OD, 293 K): δ 9.96 (d, *J* = 5.2 Hz, 1H, 39), 9.85 (d, *J* = 5.2 Hz, 1H, 49), 8.39 (m, 3H, 33,38,46), 8.33 (d, *J* = 5.3 Hz, 1H, 50), 8.25 (dd, *J* = 9.4, 3.1 Hz, 1H, 34,45), 8.03 (d, *J* = 5.6 Hz, 1H, 62), 7.91 (dd, *J* = 17.5, 7.0 Hz, 5H, 65,69,72,82,89), 7.79 – 7.63 (m, 6H, 66-68,79-81), 7.58 (m, 12H, 63,71-75,83-88), 4.73 (s, 1H, 2), 4.63 (s, 1H, 18), 4.47 (s, 1H, 53), 4.01 (d, *J* = 10.6 Hz, 5), 3.96 (d, *J* = 15.9 Hz, 1H, 5), 3.86 (d, *J* = 16.2 Hz, 1H, 24), 3.23 – 3.19 (m, 2H, 12), 3.12 – 3.08 (m, 2H, 12), 2.69 (m, 4H, 1,26), 2.22 (s, 2H, 11), 2.02-1.98 (m, 2H, 59), 1.92 (s, 2H, 91), 1.70 – 1.67 (m, 4H, 58,90), 1.62 – 1.59 (m, 3H, 22), 1.56 (s, 3H, 61), 1.51 (s, 3H, 93). **UV−vis (H_2O)**: λ_{max} in nm (ε in M^{-1} cm^{-1}) = 405 nm (1.21×10^4). **HR-MS** in CH_3CN *m/z* experimental (calcd): 707.71692 (707.71769 for $[M\text{-}2Cl]^{2+}$, $[C_{72}H_{75}N_{13}O_8RuS_2]^{2+}$), 472.14719 (472.14755 for $[M\text{-}2Cl+H]^{3+}$, $[C_{72}H_{76}N_{13}O_8RuS_2]^{3+}$).

Λ-[1]Cl_2 (8.03 mg, 5.4 µmol, 6%). **HPLC** R_T: 9.96 min (during purification). **^{1}H NMR** (850 MHz, δ in CD_3OD, 293 K): δ 9.99 (dd, *J* = 14.4, 5.3 Hz, 2H, 39,49), 8.43 – 8.36 (m, 2H, 33,38,46), 8.34 (d, *J* = 5.3 Hz, 1H, 50), 8.25 (dd, *J* = 9.4, 4.1 Hz, 2H, 34,45), 7.96 (t, *J* = 5.5 Hz, 2H, 62,89), 7.91 (t, *J* = 8.2 Hz, 4H, 68,69,78,82), 7.74 (t, *J* = 7.5 Hz, 4H, 68,68,79,81), 7.69 (t, *J* = 7.5 Hz, 2H, 67,80), 7.60 (dd, *J* = 8.6, 5.6 Hz, 2H, 63,88), 7.57 (tt, *J* = 7.7, 3.4 Hz, 10H, 71-75,83-87), 4.65 (s, 1H, 2), 4.47 (d, *J* = 7.7 Hz, 1H, 18), 4.39 (s, 1H, 53), 4.02 (s, 2H, 5), 3.86 (d, *J* = 16.6 Hz, 1H, 24), 3.20 (dt, *J* = 21.6, 7.2 Hz, 2H, 12), 2.97 (d, *J* = 16.2 Hz, 2H, 1), 2.76 (dd, *J* = 17.0, 7.7 Hz, 2H, 26), 2.29 – 2.01 (m, 5H, 11,59,91), 1.94 (d, *J* = 49.0 Hz, 4H, 58,90), 1.79 (s, 3H, 22), 1.77 (s, 3H, 61), 1.64 (s, 3H, 93). **UV−vis (H_2O)**: λ_{max} in nm (ε in M^{-1} cm^{-1}) = 405 nm (1.18×10^4). **HR-MS** in CH_3CN *m/z* experimental (calcd): 707.71689 (707.71769 for $[M\text{-}2Cl]^{2+}$, $[C_{72}H_{75}N_{13}O_8RuS_2]^{2+}$), 472.14706 (472.14755 for $[M\text{-}2Cl+H]^{3+}$, $[C_{72}H_{76}N_{13}O_8RuS_2]^{3+}$).

[Ru(Ph$_2$phen)$_2$(Ac-mrGdm-NH$_2$)]Cl$_2$ ([2]Cl$_2$)

Δ-[2]Cl_2 (10.5 mg, 7.1 µmol, 7%). **HPLC** R_T: 10.0 min (during purification). ^{1}H NMR (850 MHz, δ in CD_3OD, 293 K): δ 9.99 (dd, *J* = 11.5, 5.2 Hz, 2H, 39,49), 8.39 (m, 3H, 33,38,46), 8.34 (d, *J* = 5.1 Hz, 1H, 50), 8.25 (dd, *J* = 9.4, 5.0 Hz, 2H, 34,45), 7.96 (dd, *J* = 5.6, 2.6 Hz, 2H, 62,89), 7.90 (dd, *J* = 9.8, 7.4 Hz, 4H, 68,69,78,82), 7.75 (t, *J* = 7.5 Hz, 4H, 66,68,79,81), 7.69 (t, *J* = 7.5 Hz, 2H, 67,80), 7.61 (dd, *J* = 11.0, 5.6 Hz, 2H, 63,88), 7.57 (qt, *J* = 5.8, 3.1 Hz, 10H, 71-75,83-87), 4.66 (s, 1H, 2), 4.48 (s, 1H, 18), 4.39 (s, 1H, 53), 4.04 (d, *J* = 16.4 Hz, 1H, 5), 3.99 (s, 1H, 5), 3.86 (d, *J* = 16.7 Hz, 1H, 24), 3.22 – 3.17 (m, 2H, 12), 3.01 (dd, *J* = 17.0, 5.5 Hz, 2H, 1), 2.75 (dd, *J* = 17.0, 8.0 Hz, 2H, 26), 2.20 (dt, *J* = 14.3, 5.9 Hz, 2H, 11), 2.12 – 2.07 (m, 4H, 59,91), 2.06 – 2.01 (m, 2H, 58,90), 1.91 – 1.87 (m, 3H, 22), 1.79 (s, 3H, 61), 1.64 (s, 3H, 93). ^{13}C NMR (214 MHz, δ in CD_3OD, 293 K) δ 174.22, 172.73, 172.56, 171.97, 171.66, 169.62 (C=O, 3,6,14, 21,25,54,94), 157.17 (Cq), 153.83, 151.77, 151.42, 151.32 (CH_2), 150.68, 150.63, 150.55, 150.50, 148.80, 148.77, 147.81, 147.71, 135.68, 135.68, 135.33, 135.27 (Cq, arom), 129.99, 129.94, 129.74, 129.63, 129.61, 129.57, 129.02, 129.01, 128.94, 128.84, 128.82, 127.10, 126.91, 126.34, 126.32, 126.01 (CH, arom), 129.69, 129.59, 129.52, 129.47, 128.97, 128.91 (Cq, arom), 52.79, 51.51, 50.46, 48.08, 47,98 (CH, 2,18,24,53), 41.57, 40.47, 35.30, 32.65, 32.16, 29.90, 24.79 (CH_2, 1,11,12,26,58,59,90,91), 20.94 (CH_3, 22), 15.97 (CH_3, 61), 14.76 (CH_3, 93). **UV−vis (H_2O)**: λ_{max} in nm (ε in M^{-1} cm^{-1}) = 405 nm (1.16×10^4). **HR-MS** in CH_3CN *m/z* experimental (calcd): 707.71631 (707.71769 for $[M\text{-}2Cl]^{2+}$, $[C_{72}H_{75}N_{13}O_8RuS_2]^{2+}$), 472.14682 (472.14755 for $[M\text{-}2Cl+H]^{3+}$, $[C_{72}H_{76}N_{13}O_8RuS_2]^{3+}$).

Λ-[2]Cl_2 (12.9 mg, 8.7 μmol, 9%). HPLC R_T: 10.6 min (during purification). ^{1}H NMR (850 MHz, δ in CD_3OD, 293 K): δ 9.97 (d, *J* = 5.3 Hz, 1H, 39), 9.86 (d, *J* = 5.3 Hz, 1H, 49), 8.39 (dd, *J* = 12.1, 9.4 Hz, 3H, 33,38,46), 8.34 (dd, *J* = 14.4, 5.2 Hz, 1H, 50), 8.25 (t, *J* = 9.9 Hz, 1H, 34,45), 8.01 (d, *J* = 5.7 Hz, 2H, 62,69), 7.91 (dd, *J* = 14.8, 7.0 Hz, 4H, 65,69,78,82), 7.74 (q, *J* = 7.4 Hz, 4H, 66,68,79,81), 7.69 (dt, *J* = 10.3, 7.5 Hz, 2H, 67,80), 7.58 (m, 12H, 63,71-75,83-88), 4.51 (d, *J* = 6.9 Hz, 1H, 2), 4.67 (s, 1H, 18), 4.19 (dd, *J* = 9.0, 5.3 Hz, 1H, 53), 4.02 (t, *J* = 15.9 Hz, 2H, 5), 3.93 (d, *J* = 16.1 Hz, 1H, 24), 3.19 (ddd, *J* = 28.0, 14.3, 7.2 Hz, 2H, 12), 3.10 – 3.05 (m, 2H, 1), 2.79 (s, 2H, 26), 2.29 (d, *J* = 31.0 Hz, 2H, 11), 2.14 – 2.10 (m, 4H, 59,91), 2.10 – 2.05 (m, 4H, 58,90), 1.92 (s, 3H, 22), 1.55 (s, 3H, 61), 1.52 (s, 3H, 93). ^{13}C NMR (214 MHz, δ in CD_3OD, 293 K) δ 173.96, 172.94, 172.81, 172.34, 170.96 (C=O 3,6,14, 21,25,54,94), 157.37, 157.32 (Cq), 154.06, 153.71, 153.64, 151.40, 151.32 (CH), 150.73, 150.55, 150.51, 150.38, 148.78, 148.75, 147.78, 147.77, 135.68, 135.67, 135.30, 135.27 (Cq), 130.00, 129.98, 129.87, 129.81, 129.72, 129.66, 129.61, 129.01, 128.86, 126.32, 126.06, 126.00 (CH, arom), 129.51, 129.46, 128.90, 128.88 (Cq, arom), 55.08, 53.18, 52.75, 47.91 (CH, 2,18,24,53), 46.44, 43.83, 40.56, 31.20, 25.57 (CH_2, 1,11,12,26,58,59,90,91), 21.16 (CH_3, 22), 14.60 (CH_3, 61), 14.35 (CH_3, 93). **UV−vis (H_2O)**: λ_{max} in nm (ε in M^{-1} cm^{-1}) = 405 nm (1.27×10^4). **HR-MS** in CH_3CN *m/z* experimental (calcd): 707.71662 (707.71769 for $[M\text{-}2Cl]^{2+}$, $[C_{72}H_{75}N_{13}O_8RuS_2]^{2+}$), 472.14711 (472.14755 for $[M\text{-}2Cl+H]^{3+}$, $[C_{72}H_{76}N_{13}O_8RuS_2]^{3+}$).

[Ru(Ph₂phen)₂(Ac-MrGdM-NH₂)]Cl₂ ([3]Cl₂)

Δ-[3]Cl_2. (1.58 mg, 1.1 μmol, 2%). **HPLC** R_T: 10.2 min (during purification). **^{1}H NMR** (850 MHz, δ in CD_3OD, 293 K): δ 9.94 (d, *J* = 5.1 Hz, 1H, 39), 9.83 (d, *J* = 5.4 Hz, 1H, 49), 8.51 (d, *J* = 5.3 Hz, 1H, 50), 8.36 (dt, *J* = 14.0, 8.0 Hz, 3H, 33,38,46), 8.24 (t, *J* = 9.7 Hz, 2H, 34,45), 7.94 – 7.87 (m, 6H, 62,65,68,79,81,89), 7.74 (dd, *J* = 15.1, 7.6 Hz, 4H, 66,68,79,81), 7.72 – 7.66 (m, 2H, 67,80), 7.56 (m, 10H, 71-75, 83-87), 4.23 (s, 1H, 18), 4.20 (s, 1H, 53), 4.08 (d, *J* = 16.7 Hz, 2H, 5), 3.93 (d, *J* = 17.0 Hz, 2H, 2,24), 2.99 (d, *J* = 17.1 Hz, 1H, 12), 2.96 (s, 1H, 12), 2.71 – 2.67 (m, 2H, 1), 2.63 (s, 2H, 26), 2.47 (s, 2H, 11), 2.11 (s, 4H, 58,59,90,91), 1.71 (s, 3H, 22), 1.53 (s, 6H, 61,93). ^{13}C NMR (214 MHz, δ in CD_3OD, 293 K) δ 172.31, 172.14, 172.08, 171.78, 168.58 (C=O, 3,6,14, 21,25,54,94), 156.34 (Cq) 153.08, 150.38 (CH), 149.87, 149.82, 149.57, 149.52, 147.92, 146.89, 146.78, 134.75, 134.72, 134.42, 134.37 (Cq, arom), 129.18, 129.01, 128.88, 128.74, 128.70, 128.65, 128.13, 128.02, 127.95, 126.58, 126.10, 125.44, 125.41, 125.15, 125.01 (CH, arom), 53.69, 52.91, 52.68, 49.05 (CH, 2,18,24,53), 42.76, 39.63, 32.13, 30.14, 28.17, 28.07, 25.14 (CH_2, 1,11,12,26,58,59,90,91), 20.56 (CH_3, 22), 14.90

(CH_3, 61), 14.27 (CH_3, 93). **UV−vis (H_2O)**: λ_{max} in nm (ε in M^{-1} cm^{-1}) = 405 nm (1.05×10^4). **HR-MS** in CH_3CN *m/z* experimental (calcd): 707.71711 (707.71769 for $[M\text{-}2Cl]^{2+}$, $[C_{72}H_{75}N_{13}O_8RuS_2]^{2+}$), 472.14722 (472.14755 for $[M\text{-}2Cl+H]^{3+}$, $[C_{72}H_{76}N_{13}O_8RuS_2]^{3+}$).

Λ-[3]Cl_2 (3.18 mg, 2.1 µmol, 4%). **HPLC** R_T: 11.4 min (during purification). ^{1}H NMR (850 MHz, δ in CD_3OD, 293 K):^{1}H NMR (850 MHz, δ in CD_3OD, 293 K) δ 9.94 (d, *J* = 5.3 Hz, 1H, 39), 9.85 (d, *J* = 5.3 Hz, 1H, 49), 8.41 (dd, *J* = 9.4, 5.1 Hz, 2H, 33,46), 8.33 (d, *J* = 5.3 Hz, 1H, 50), 8.27 (dd, *J* = 9.4, 2.9 Hz, 2H, 34,35), 7.99 (d, *J* = 5.6 Hz, 1H, 62), 7.95 (d, *J* = 5.6 Hz, 1H, 89), 7.92 (dd, *J* = 17.2, 7.4 Hz, 4H, 65,69,78,82), 7.76 (td, *J* = 7.7, 1.9 Hz, 4H, 66,68,79,81), 7.74 – 7.72 (m, 2H, 67-80), 7.71 – 7.65 (m, 2H, 63,88), 7.62 – 7.54 (m, 10H, 71-75,83-87), 4.51 (t, *J* = 4.2 Hz, 1H, 2), 4.24 (dd, *J* = 9.0, 5.1 Hz, 1H, 18), 4.13 (s, 1H, 53), 4.05-4.01 (dd, *J* = 16.6, Hz, 2H, 5), 3.95 (t, *J* = 7.7 Hz, 1H, 24), 3.22 – 3.18 (m, 2H, 12), 3.02 (dd, *J* = 17.2, 3.4 Hz, 1H, 1), 2.59 (dd, *J* = 17.1, 5.1 Hz, 1H, 26), 2.42 (s, 1H), 2.23 (dt, *J* = 13.1, 6.4 Hz, 2H, 11), 2.12 (s, 4H, 59,91), 2.00 (s, 4H, 58,90), 1.75 (s, 3H, 22), 1.58 (ds, 6H, 61,93). ^{13}C NMR (214 MHz, MeOD) δ 177.09, 174.40, 173.15, 172.95, 172.13, 170.25 (C=O, 3,6,14, 21,25,54,94), 157.47 (Cq), 151.04, 151.23 (CH), 150.77, 150.69, 150.55, 150.48, 148.80, 148.75, 147.78, 147.74 (Cq, arom), 135.70, 135.66, 135.28, 135.28 (Cq, arom), 129.81, 129.67, 129.59, 129.50, 129.48, 129.14, 128.90, 127.04, 126.30, 125.97 (CH, arom), 54.74, 53.81, 52.95, 50.42 (CH, 2,18,24,53) 40.87, 37.44, 33.28, 32.15, 29.83, 29.25, 25.22 (CH_2, 1,11,12,26,58,59,90,91), 20.79 (CH_3, 22), 15.17 (CH_3, 61,93). **UV−vis (H_2O)**: λ_{max} in nm (ε in M^{-1} cm^{-1}) = 405 nm (1.12×10^4). **HR-MS** in CH_3CN *m/z* experimental (calcd): 707.71668 (707.71769 for $[M\text{-}2Cl]^{2+}$, $[C_{72}H_{75}N_{13}O_8RuS_2]^{2+}$), 472.14702 (472.14755 for $[M\text{-}2Cl+H]^{3+}$, $[C_{72}H_{76}N_{13}O_8RuS_2]^{3+}$). .

5.5.3 Cellular uptake

The intracellular ruthenium uptake by A549 and PC-3 cells was assessed by ICP-MS. Normoxic and hypoxic cells from both cell lines were seeded in 100 µL Opti-MEM at a density of 5×10^3 (A549) or 6×10^3 (PC-3) cells in black 96-well plates. After 24 h, 100 µL of 10 µM drug solution in OptiMEM was added in sextuplicate to A549 cells as well as to PC-3 cells. 12 wells per plate were filled with 100 µL Opti-MEM for control. After another 24 h incubation in the dark, the drug-containing medium was removed, cells were washed once (150 µL for each well) with phosphate buffered saline (PBS), and stained with 50 µL Nuclear Blue (2 drops per mL OptiMEM, Fischer scientific R37605) for 30 min. Subsequently, the excess dye was removed, fresh medium was added, and each well was captured by Nikon TiE2000 confocal laser microscope. Data processing by Image-Pro Analyzer 7.0 resulted in the cell number per well. After imaging, all medium was removed, and the cells were lysed by adding 100 µL 65% HNO_3

(1.00441.1000, Sigma) per well. The lysate was diluted by adding 900 µL MilliQ water (10 × dilution) in a deep well plate (Eppendorf, E951033502), and the ruthenium content of every 1 mL well was determined by ICP-MS (PerkinElmer NexION 2000) in ppb (µg/L). In Microsoft Excel 365, the ruthenium uptake values were calculated in µg Ru /million cells by dividing the determined Ru content per well in µg by the number of counted cells per well. Mean values (n=6) and standard deviation were reported in Figure 5.3a. Significance between data sets were calculated in Microsoft Excel 365 by a two-sample unequal variance Student's t-Test using a two-tailed distribution.

5.5.4 Viability assay of 3D tumor spheroids

A549 cells (700) were added to a 96-well round-bottomed Corning spheroid plate (Catalogue CLS4520) microplate and incubated under normoxia (21% O_2) for 4 days to generate 3D tumor spheroids. Spheroids were grown in 100 µL Opti-MEM (Gibco complete medium 11058-021, supplemented with 2.5% v/v fetal calf serum (FCS), 0.2% v/v penicillin/streptomycin (P/S), and 1% v/v glutamine). 1 dark and 1 light plate was included in one group. After that, 100 µL of different concentrations of **[1]**Cl_2**-[2]**Cl_2 dissolved in Opti-MEM were added to each well in triplicate to reach final concentrations in the wells of 0, 1, 2.5, 5, 10, 25, 50 and 100 µM. The spheroids were incubated further under normoxia for 24 h. Then, the light plate was irradiated with green light for 30 min (dose = 13.1 J/cm^2, wavelength = 520 nm, intensity = 7.22 mW/cm^2), and the other plate was left in the dark. The cells were further incubated under normoxia in the dark for 2 days, a CellTiter Glo 3D solution (100 µL/well, Cat. G9683, Promega, no further dilution) was added to each well (to 300 µL final volume) to stain the 3D tumor spheroids. After 30 min of shaking on an IKA Vibrax shaker at 500 rpm at room temperature, the luminescence (560 nm) in each well was measured with a Tecan microplate reader. Similar to 2D cell cultures, half-maximal effective concentrations (EC_{50}) for 3D tumor spheroid growth inhibition were calculated by Graphpad Prism 5 using the dose-response two-parameter Hill slope equation (Equation AI.3). All experiments were conducted in biologically independent triplicate.

5.6 References

1. K. Graham and E. Unger, *International journal of nanomedicine*, 2018, **13**, 6049.
2. P. Vaupel, A. Mayer and M. Höckel, in *Methods in enzymology*, Elsevier, 2004, vol. 381, pp. 335-354.
3. D. M. Gilkes, G. L. Semenza and D. Wirtz, *Nature Reviews Cancer*, 2014, **14**, 430-439.
4. G. L. Semenza, *Annual Review of Pathology: Mechanisms of Disease*, 2014, **9**, 47-71.
5. H. D. Cole, J. A. Roque III, G. Shi, L. M. Lifshits, E. Ramasamy, P. C. Barrett, R. O. Hodges, C. G. Cameron and S. A. McFarland, *Journal of the American Chemical Society*, 2021, **144**, 9543-9547.
6. P. Agostinis, K. Berg, K. A. Cengel, T. H. Foster, A. W. Girotti, S. O. Gollnick, S. M. Hahn, M. R. Hamblin, A. Juzeniene and D. Kessel, *CA: a cancer journal for clinicians*, 2011, **61**, 250-281.
7. X. Li, J. F. Lovell, J. Yoon and X. Chen, *Nature Reviews Clinical Oncology*, 2020, **17**, 657-674.

8. F. E. Poynton, S. A. Bright, S. Blasco, D. C. Williams, J. M. Kelly and T. Gunnlaugsson, *Chemical Society Reviews*, 2017, **46**, 7706-7756.
9. L. N. Lameijer, D. Ernst, S. L. Hopkins, M. S. Meijer, S. H. Askes, S. E. Le Dévédec and S. Bonnet, *Angewandte Chemie*, 2017, **129**, 11707-11711.
10. J.-A. Cuello-Garibo, M. S. Meijer and S. Bonnet, *Chemical Communications*, 2017, **53**, 6768-6771.
11. N. J. Farrer, L. Salassa and P. J. Sadler, *Dalton Transactions*, 2009, 10690-10701.
12. S. Bonnet, *Dalton Transactions*, 2018, **47**, 10330-10343.
13. Y. Liu, R. Hammitt, D. A. Lutterman, L. E. Joyce, R. P. Thummel and C. Turro, *Inorganic chemistry*, 2008, **48**, 375-385.
14. K. M. Mahmud, M. S. Niloy, M. S. Shakil and M. A. Islam, *Pharmaceutics*, 2021, **13**, 1295.
15. Y. Chen, L. Bai, P. Zhang, H. Zhao and Q. Zhou, *Molecules*, 2021, **26**, 5679.
16. T. N. Singh and C. Turro, *Inorganic chemistry*, 2004, **43**, 7260-7262.
17. D. V. Pinnick and B. Durham, *Inorganic Chemistry*, 1984, **23**, 1440-1445.
18. Y. Liu, D. B. Turner, T. N. Singh, A. M. Angeles-Boza, A. Chouai, K. R. Dunbar and C. Turro, *Journal of the American Chemical Society*, 2009, **131**, 26-27.
19. V. H. van Rixel, V. Ramu, A. B. Auyeung, N. Beztsinna, D. Y. Leger, L. N. Lameijer, S. T. Hilt, S. E. Le Dévédec, T. Yildiz and T. Betancourt, *Journal of the American Chemical Society*, 2019, **141**, 18444-18454.
20. R. N. Garner, L. E. Joyce and C. Turro, *Inorganic Chemistry*, 2011, **50**, 4384-4391.
21. Y. Zheng, Q. Zhou, W. Lei, Y. Hou, K. Li, Y. Chen, B. Zhang and X. Wang, *Chemical Communications*, 2015, **51**, 428-430.
22. M. Kayanuma, M. Shoji and Y. Shigeta, *The Journal of Physical Chemistry A*, 2019, **123**, 2497-2502.
23. K. Szaciłowski, W. Macyk, A. Drzewiecka-Matuszek, M. Brindell and G. Stochel, *Chemical reviews*, 2005, **105**, 2647-2694.
24. R. N. Garner, L. E. Joyce and C. Turro, *Inorganic Chemistry*, 2011, **50**, 4384-4391.
25. J. F. Machado, J. D. G. Correia and T. S. Morais, *Molecules*, 2021, **26**, 3153.
26. F. Barragán, P. López-Senín, L. Salassa, S. Betanzos-Lara, A. Habtemariam, V. Moreno, P. J. Sadler and V. Marchán, *Journal of the American Chemical Society*, 2011, **133**, 14098-14108.
27. A. Gandioso, E. Shaili, A. Massaguer, G. Artigas, A. González-Cantó, J. A. Woods, P. J. Sadler and V. Marchán, *Chemical Communications*, 2015, **51**, 9169-9172.
28. S. Chakrabortty, B. K. Agrawalla, A. Stumper, N. M. Vegi, S. Fischer, C. Reichardt, M. Kögler, B. Dietzek, M. Feuring-Buske and C. Buske, *Journal of the American Chemical Society*, 2017, **139**, 2512-2519.
29. O. H. Aina, T. C. Sroka, M. L. Chen and K. S. Lam, *Peptide Science: Original Research on Biomolecules*, 2002, **66**, 184-199.
30. M. Kalmouni, S. Al-Hosani and M. Magzoub, *Cellular and Molecular Life Sciences*, 2019, **76**, 2171-2183.
31. M. Muttenthaler, G. F. King, D. J. Adams and P. F. Alewood, *Nature reviews Drug discovery*, 2021, **20**, 309-325.
32. S. S. Kale, C. Villequey, X.-D. Kong, A. Zorzi, K. Deyle and C. Heinis, *Nature chemistry*, 2018, **10**, 715-723.
33. M. Muttenthaler, A. Andersson, A. D. de Araujo, Z. Dekan, R. J. Lewis and P. F. Alewood, *Journal of medicinal chemistry*, 2010, **53**, 8585-8596.
34. B. Yoo and K. Kirshenbaum, *Current opinion in chemical biology*, 2008, **12**, 714-721.
35. F. Fülöp, T. A. Martinek and G. K. Tóth, *Chemical Society Reviews*, 2006, **35**, 323-334.
36. T. van Groen, S. Schemmert, O. Brener, L. Gremer, T. Ziehm, M. Tusche, L. Nagel-Steger, I. Kadish, E. Schartmann and A. Elfgen, *Scientific reports*, 2017, **7**, 16275.
37. S. Nakano, S. Okazaki, E. Ishitsubo, N. Kawahara, H. Komeda, H. Tokiwa and Y. Asano, *Scientific Reports*, 2015, **5**, 1-12.
38. G. Genchi, *Amino Acids*, 2017, **49**, 1521-1533.
39. S. A. Funke and D. Willbold, *Molecular BioSystems*, 2009, **5**, 783-786.
40. X. Wei, C. Zhan, Q. Shen, W. Fu, C. Xie, J. Gao, C. Peng, P. Zheng and W. Lu, *Angewandte Chemie*, 2015, **127**, 3066-3070.
41. D. M. Rogers, S. B. Jasim, N. T. Dyer, F. Auvray, M. Réfrégiers and J. D. Hirst, *Chem*, 2019, **5**, 2751-2774.
42. K. Naing, M. Takahashi, M. Taniguchi and A. Yamagishi, *Inorganic Chemistry*, 1995, **34**, 350-356.
43. B. Bosnich, *Accounts of Chemical Research*, 1969, **2**, 266-273.
44. J. Fan, J. Autschbach and T. Ziegler, *Inorganic Chemistry*, 2010, **49**, 1355-1362.
45. M. S. Meijer, Leiden University, 2018.
46. K. Eastham, P. A. Scattergood, D. Chu, R. Z. Boota, A. Soupart, F. Alary, I. M. Dixon, C. R. Rice, S. J. Hardman and P. I. Elliott, *Inorganic Chemistry*, 2022, **61**, 19907-19924.
47. M. C. DeRosa and R. J. Crutchley, *Coordination Chemistry Reviews*, 2002, **233**, 351-371.
48. S. E. Ackerman, C. M. Wilson, S. A. Kahn, J. R. Kintzing, D. A. Jindal, S. H. Cheshier, G. A. Grant and J. R. Cochran, *Cureus*, 2014, **6**.
49. F. Danhier, A. Le Breton and V. r. Préat, *Molecular pharmaceutics*, 2012, **9**, 2961-2973.
50. J. A. Ju, I. Godet, I. C. Ye, J. Byun, H. Jayatilaka, S. J. Lee, L. Xiang, D. Samanta, M. H. Lee and P.-H. Wu, *Molecular Cancer Research*, 2017, **15**, 723-734.
51. K. D. Cowden Dahl, S. E. Robertson, V. M. Weaver and M. C. Simon, *Molecular biology of the cell*, 2005, **16**, 1901-1912.
52. B. A. Teicher, J. S. Lazo and A. C. Sartorelli, *Cancer research*, 1981, **41**, 73-81.
53. B. A. Teicher, S. A. Holden, A. Al-Achi and T. S. Herman, *Cancer research*, 1990, **50**, 3339-3344.
54. B. LaFoya, J. A. Munroe, A. Miyamoto, M. A. Detweiler, J. J. Crow, T. Gazdik and A. R. Albig, *International journal of molecular sciences*, 2018, **19**, 449.

55. V. Vichai and K. Kirtikara, *Nature protocols*, 2006, **1**, 1112-1116.
56. E. C. Costa, A. F. Moreira, D. de Melo-Diogo, V. M. Gaspar, M. P. Carvalho and I. J. Correia, *Biotechnology advances*, 2016, **34**, 1427-1441.
57. A. Zorzi, S. J. Middendorp, J. Wilbs, K. Deyle and C. Heinis, *Nature Communications*, 2017, **8**, 16092.